Article

Use of the Retinal Vascular Histology to Validate an Optical Coherence Tomography Angiography Technique

Paula K. Yu[1,2], Andrew Mehnert[3,4], Arman Athwal[2,5], Marinko V. Sarunic[5], and Dao-Yi Yu[1,2]

[1] Centre for Ophthalmology and Visual Science, University of Western Australia, Perth, Australia
[2] Lions Eye Institute, Nedlands, Western Australia, Australia
[3] Centre for Microscopy Characterisation and Analysis, University of Western Australia, Perth, Australia
[4] National Imaging Facility, Australia
[5] School of Engineering Science, Simon Fraser University, Burnaby, BC, Canada

Correspondence: Dao-Yi Yu, Centre for Ophthalmology and Visual Science, The University of Western Australia, Nedlands, 6009, Western Australia.
e-mail: dyyu@lei.org.au

Purpose: To determine the fidelity of optical coherence tomography angiography (OCTA) techniques by direct comparison of the retinal capillary network images obtained from the same region as imaged by OCTA and high-resolution confocal microscope.

Method: Ten porcine eyes were perfused with red blood cells for OCTA image acquisition from the area centralis and then perfusion-fixed, and the vessels were labeled for confocal imaging. Two approaches involving post-processing of two-dimensional projection images and vessel tracking on three dimensional image stacks were used to obtain quantitative measurements. Data collected include vessel density, length of visible vessel track, count of visible branch points, vessel track depth, vessel diameter, angle of vessel descent, and angle of dive for comparison and analysis.

Results: Comparing vascular images acquired from OCTA and confocal microscopy, we found (1) a good representation of the larger caliber retinal vessels, (2) an underrepresentation of retinal microvessels smaller than 10 μm and branch points in all four retinal vascular plexuses, particularly the intermediate capillary plexus, (3) reduced visibility associated with an increase in the angle of descent, (4) a tendency to loss visibility of vessel track at a branch point or during a sharp dive, and (5) a reduction in visibility with increase in retinal depth on OCTA images.

Conclusions: Current OCTA techniques can visualize the retinal capillary network, but some types of capillaries cannot be detected by OCTA, particularly in the middle to deeper layers.

Translational Relevance: The information indicates the limitation in clinical use and scopes for improvement in the current OCTA technologies.

Introduction

Optical coherence tomography angiography (OCTA) has been widely used clinically as a powerful tool to visualize the retinal capillary network in living subjects noninvasively and without the need of a contrast agent. It provides a volume imaging tool that allows further understanding of the normative human retinal vascular anatomy and physiology, displays pathological and disease progression,[1] and has a higher specificity and sensitivity in detecting some ocular vasculopathies.[2,3]

However, image artifacts in OCTA have been noted and could produce some confusing information.[1,4,5] An obvious example is the wide range of measurements in macular vessel density where 27.6% to more than 90.0% has been reported in various studies using OCTA techniques.[6–8] However, a recent quantitative vascular histological study from our group[9] on the density of the human macular vasculature confirmed the lower range to be closer to the truth. This poses

a question on the reliability of the quantitative data currently being reported from OCTA techniques and often used for clinical interpretation. Hence, there is a need for OCTA techniques to be properly validated.

One of the most reliable validation methods is to directly compare retinal vascular histology with OCTA images from the same region in the same eye. We have studied retinal vascular histology using microperfusion and labeling techniques for more than 10 years and demonstrated that the intact retinal capillary network can be reliably obtained as a gold standard to validate OCTA images.[10–14] Although we attempted a direct histology and OCTA comparison in a human case,[15] that study was limited by the sample number and poor quality of images obtained.

To properly validate OCTA, this study uses isolated arterially perfused porcine eyes as the model from which OCTA and histological data can be obtained from the exact same retinal region for direct comparison and assessment. In addition to good quality of OCTA images from fresh eyes, motion artefacts in the OCTA images can be avoided.

Materials and Methods

All experiments were conducted in accordance with the ARVO Statement for the Use of Animals in Ophthalmic and Vision Research. The study was approved by the University of Western Australia Animal Welfare Office. Expired human red blood cells were obtained from the Australia Red Cross Blood Service under a material supply deed.

Isolated Arterially Perfused Eye Preparation

Ten freshly enucleated pig eyes were obtained from the local abattoir and transported in ice-cold carbogen-bubbled Ringer's solution in gas-tight containers to the laboratory within an hour of enucleation and stored in the laboratory fridge before use. The isolated arterially perfused eye preparation was similar to our previous reports[10–14,16,17] and will be briefly described here.

Extraocular muscles and connective tissues surrounding the globe and the optic nerve were carefully dissected out and the cornea protected from dehydration using a hard contact lens and a drop of GelTeal Gel (Alcon, Geneva, Switzerland). The superoinferior orientation of the porcine eye was determined on the basis of the positions of the two ciliary arteries and position of the three major retinal arteries as observed through the cornea and plano-concave contact lens under an operating micro-

scope. The porcine eye is a good model for this study because it is similar to the human eye in having a fully vascularized retina,[18] is of similar anatomical size,[19] and can be reliably sourced fresh from the local abattoir. The retinal vasculature was perfused using red blood cells for OCTA image acquisition and then perfusion labeled for confocal imaging. The use of an isolated porcine eye securely seated in a custom-made eye holder eliminated any confounding effect of motion artefacts, a major advantage over scanning live subjects.

The chorioretinal arteries running along the optic nerve sheath to supply the superior hemisphere of the porcine retina were carefully dissected out using blunt dissection on the surrounding adipose tissues. The supplying artery branch that is located closest to the superior retinal artery is cannulated as close to the optic nerve head as possible.

The chorioretinal artery was cannulated using a glass pipette with a tip size around 120 to 160 μm and perfused with heparinized Ringer's solution (100 U/10 mL) to wash out the red blood cells. Clearing of residual red blood cells from the retinal vessels was confirmed visually using the plano-concave lens and the operating microscope as previously described.[20] The perfusate was then changed to a mixture of two parts expired human red blood cells in one part heparinized Ringer's solution as hematocrit of around 40%, which is similar to the normal range for OCTA imaging at a typical flow rate of 800 μL/min.

OCTA Imaging and Region of Interest

The device used in this study was a custom-built swept source OCT (SS-OCT) system described previously.[21] The rationale to use this device is that it has a faster acquisition capability than current commercially available OCT and that each image processing step is known. Using this device, we could reliably determine the limitations of the different OCTA acquisition techniques. Briefly, the 1060 nm SS-OCT system used a 200 kHz swept source (Axsun Technology Inc., Billerica, MA, USA) with a full-width half maximum (FWHM) spectrum of 80 nm. The digitized spectrum used for imaging granted an approximate axial resolution of ~4.5 μm in tissue (based on the most accepted refractive index of tissue, n = 1.38). The beam diameter incident on the cornea and spot size at a retina were approximately 1.6 mm and 13 μm, respectively. The average power of the OCT imaging beam on the cornea was configured to be below 1.5 mW to satisfy the maximum permission ocular exposure as defined by ANSI Z136.1 (2014) safety limits.[22] The transversal area of 1.5 mm (horizontal) by ~1.5 mm

(vertical) was scanned with either a 400 height × 1200 frames (3 BM) or 400 height × 2000 frames (5 BM) OCTA scanning protocol, resulting in volume acquisition times of 2.4 seconds or 4.0 seconds, respectively. The images were taken at a single location using step bidirectional scanning in which the slow scan axis is stepped at the B-scan frequency to obtain a constant time interval between the two B-scans and without laser fly-back.[21]

The OCTA device was positioned to aim at the area centralis/foveal streak[19] located in the dorsal hemisphere, an area measuring approximately 1.5 mm^2 that is rich in capillaries supplied by a retinal arteriole and away from the major retinal arteries and veins. Screen shots were taken of the en face projection (either a maximum-intensity projection or mean-intensity projection) of the area being imaged to enable matching of the region of interest during confocal imaging. Twenty volumes were acquired 3.5 seconds apart and then averaged voxel-wise, and the resulting volume saved as a stack of en face projection images in a multi-image TIFF file for further analysis. Each image is an en face maximum intensity or mean intensity projection of 2.5 µm. The pixel size in the 10 stacks ranges from 3.85 µm to 4.14 µm.

Twenty volumes were acquired sequentially per experiment. After acquisition, standard swept source-OCT processes such as wavenumber resampling, numerical dispersion compensation, and fast Fourier transform was performed on the acquired raw OCT data. The OCT-A microvascular signal was extracted from the complex OCT data via an absolute complex difference OCT-A technique.[23] A three-dimensional (3D) bounded variance smoothing was applied to the motion-corrected OCT intensity B-scans to enhance the boundaries between retinal layers and aid layer segmentation. The posterior boundary of the outer nuclear layer (ONL) was automatically segmented from the smoothed OCT data in 3D using a graph-cut algorithm.[24] The 3D OCT-A volumes were flattened with respect to the ONL segmentation. Each set of 20 OCT-A volumes was averaged across time to create a single, high-contrast vascular flow cube that was subsequently saved as a 3D TIFF stack for visualization.

Fixation, Labeling, and Confocal Imaging

After OCTA image acquisition was completed, the retinal vasculature was immediately perfusion fixed using 4% paraformaldehyde in 0.1 M phosphate buffer through the same chorioretinal artery that had already been cannulated for red blood cells perfusion. The microvasculature was perfusion-labeled using Lectins-FITC (P5282; Sigma-Aldrich Corp., St. Louis,

MO, USA) or Lectins-TRITC (P1951; Sigma-Aldrich Corp.) using methodology previously described.[9,20,25] One porcine eye was labeled for calponin using antibodies (ab46794; Abcam, Cambridge, MA, USA) using protocol previously described.[26] After labeling, the porcine eye was cut open at the equator to remove the anterior chamber, the lens, and the vitreous. The posterior globe with the retina attached to it was immerse fixed overnight in 4% paraformaldehyde at 4°C. The perfuse-labeled retina was detached from the globe and spread onto a glass slide with radial cuts to the periphery and flat mounted in a few drops of RapidClear (Sunjin Lab Co., Hsinchu City, Taiwan) to enhance fluoroprobe visibility.

Confocal images were acquired using a Nikon C1 Plus system (Nikon Inc., Melville, NY, USA) coupled with Nikon Integrated Software (NIS) elements software. The exact location of the region of interest on the retinal flat mount was identified with the aid of the en face screen shot from the OCTA volume acquisition. Stacks of two-dimensional (2D) images were acquired through the retinal thickness at an optical thickness of 1.25 to 6.25 µm apart containing labeled microvasculature using the ×4 and ×10 Plan Apo objective lenses centered on the OCTA imaged region and saved as multi-image TIFF files.

Image Analysis Approaches Used for Comparison Between Corresponding OCTA and Confocal Image Stacks

Two image analysis approaches, one based on 2D projections and the other on 3D volume renderings, were used to quantitatively compare pairs of corresponding OCTA and confocal image stacks. The analyses were performed using FIJI[27] (V1.52p) and Imaris (V7.5.2; Bitplane AG, Zurich, Switzerland).

Approach Based on 2D Projections from the Four Vascular Layers

In this approach, 2D projections (either maximum or mean intensity) of the four retinal vascular layers,[28,29] namely (1) the radial peripapillary capillary network (RPCN), (2) the superficial vascular plexus (SVP), (3) the intermediate capillary plexus (ICP), and (4) the deep capillary plexus (DCP) were made from the confocal and OCTA image stacks and saved as single-image TIFF files. Corresponding pairs of OCTA and confocal 2D projections at each layer were then processed as follows.

Pre-Processing to Detect Vessel Centerlines and Globally Co-Register the Centerline Images. A FIJI script (see Supplementary material) was written to the following:

1. Apply a nonlocal means filter to the OCTA image to attenuate noise;
2. Detect different caliber blood vessels in both the denoised OCTA and confocal images. For each image this is achieved by applying a tubeness filter (https://www.longair.net/edinburgh/imagej/tubeness/) independently at multiple size scales (two sizes for the OCTA image and five sizes for the higher-resolution confocal image) and computing the pixel-wise maximum of the results;
3. Detect vessel centerlines/ridges (https://imagej.net/Ridge_Detection) in these images; and
4. Globally align (translation, scaling and rotation) the OCTA ridge image to the confocal ridge image.

Pairwise Comparisons of Vessels Based on Grid-Line Intercepts. A FIJI script (see Supplementary material) was written to superimpose evenly spaced pairs of vertical and horizontal grid lines on each pair of preprocessed images, and for each line to count the number of vessel ridge lines that intersect the line. From this it is possible to calculate the number of vessels per 100 μm of the grid line in each image, a measure previously used in comparing vessel density in the human retina.[11,12,30] The intercapillary distance is an inversion of this index and provides an estimate of how far apart the vessels are in each vascular layer.[11,30]

Pairwise Comparisons of Vessels Based on Elastic Matching. The FIJI bUnwarpJ plugin[31] was applied (see Supplementary material) to each pair of preprocessed images to elastically register the OCTA ridge image to the confocal ridge image (optionally assisted by user placed landmarks). For image pairs from ICP where there was a lack of visually comparable structures, the transformation previously calculated for the SVP or DCP was applied. A custom-written FIJI script (see Supplementary material) was then used to dilate both the confocal and coregistered OCTA ridge images (to compensate for center-line wiggle) and calculate the number of pixels in common and unique to each.

3D Approach

The 2D approach enables the quantitative comparison of a pair of OCTA and confocal images from the same layer in terms of the density of vessels (or more precisely, projected vessel centerlines), and of the vessel structures in common and unique to each. However, it does not quantify in 3D what specific vessels in the confocal stack (the ground truth) can be seen in the 3D stack. To address this, a region-of-interest (ROI) measuring 800×500 μm in the transverse plane and containing an arteriole branch stemming from the major retinal artery was selected from each specimen (Fig. 1). Four to five vessels branching off this arteriole were traced in both the confocal and OCTA image stacks side-by-side in FIJI using the multi-point tool, together with the ROI manager, to record the 3D coordinates of each track point. Imaris was then used to (i) volume render the confocal stack and to trace both the confocal and OCTA paths guided by the FIJI results and (ii) compute the length of each track, depth of track travel, the number of branch points visible, diameter of the vessel at the end of the visible track, and the angle of dive for vessels traveling into the deeper retina. The angle of dive is defined as a sharp downward descent of the vessel track into the deeper retina along part of the track. If (x_1,y_1,z_1) denotes the coordinates at the start of the dive and (x_2,y_2,z_2) denotes the coordinates at the end, then the angle of descent is given by arctan of the division of the absolute value of the difference $z_1 - z_2$, by the Euclidean distance between (x_1,y_1) and (x_2,y_2), that is, $\theta = \tan^{-1}(|z_1 - z_2|/\sqrt{(x_1 - x_2)^2 + (y_1 - y_2)^2})$. Specific features associated with the loss of vessel track on OCTA were also recorded.

Grouping of Vessel Tracks. The vessel tracks were further grouped according to the angle of vessel descent. The angle of (vessel) descent is computed in the same way as the angle of dive, but with (x_1,y_1,z_1) and (x_2,y_2,z_2) as the start and end of the vessel track, respectively. The vessels were further segregated into three groups with distinct conditions as follows:

- Group A: Vessel track stays within the most superficial retinal vessel layer within 20 μm in total track depth travel; no sudden dive of the vessel track into the deeper retina
- Group B: Part of the vessel track makes a sharp descent ($>30°$) into the deeper retina
- Group C: Gradual descent ($<30°$) of the track into the deeper retina but no sharp dive along the track

Data Analysis

The measurements obtained were analyzed using the statistical package SigmaPlot (Version 12.5, Systat Software, Inc., San Jose, CA, USA). Ridge line pixel counts, vessel density counts by grid line intercepts, vessel track length, the number of branch points along vessel tracks obtained from corresponding confocal and OCTA images, and vessel track depth were compared using paired *t*-tests. Differences in measurements between vascular layers were analyzed using
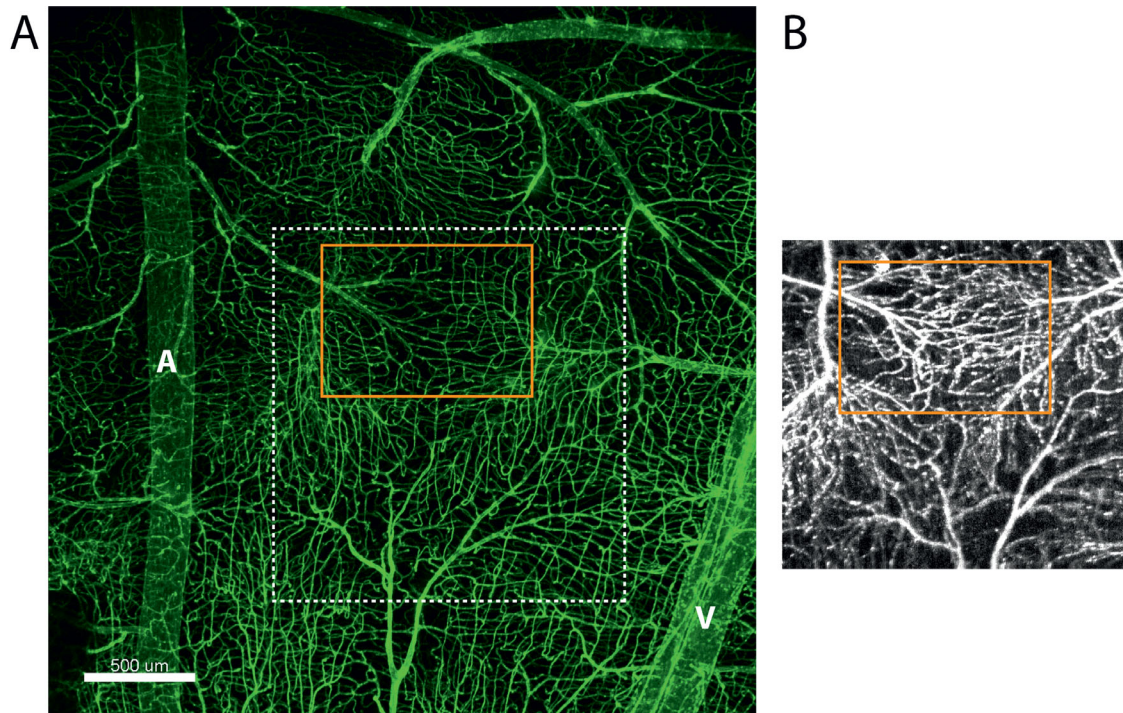
Figure 1. ROI. (A) A 2D maximum-intensity projection through a confocal stack taken from a lectin-FITC–labeled retinal microvasculature of the superior hemisphere in a porcine retina; taken at low magnification (×4) and centering on a typical study region as outlined by the orange rectangular frame. *A* denotes a major retinal artery, whereas *V* denotes a major retinal vein. The ROI measures 800 µm × 500 µm in area and contains an arteriole branch coming in from the left-hand side of the frame and draining out towards retinal vein on the right hand side. The region within the dotted white lines correspond to the area scanned using OCTA technique. (B) The 2D projected OCTA image stack taken from the corresponding region of interest of this pig retina. The study region in the OCTA projected image is also outlined using an orange rectangle. *Scale bar:* 500 µm.

one-way analysis of variance (ANOVA) using the layer name as the factor in consideration. Differences in angle measurements of the three vessel groups were compared using one-way ANOVA using grouping name as the factor in consideration.

Results

Qualitative observations and quantitative measurements were obtained using the different approaches.

Qualitative Observations

Projection Artefact from Large Retinal Vessels on OCTA

Side-by-side comparisons of 2D maximum intensity or mean intensity projections of the image stacks acquired from the same region using confocal and OCTA techniques show that the latter closely resembles the appearance of the vascular network on histologic preparations, especially the orientation and branching of major retinal arteries and veins. Figure 2 shows one set of data demonstrating the general overall resemblance of the OCTA image stack to the confocal image stack. When segregated into top and bottom halves for comparison, it became apparent that the major retinal arteries and veins which are only present in a specific layer of the confocal z-stack were visible through the thickness of the OCTA z-stack, reflecting the presence of projection artefacts in the OCTA technique.

Absence of Small Vessels in the ICP on OCTA Images

Further segregation of the image stacks into thinner layers, as in Figure 3, revealed an absence of small retinal vessels from all layers. In particular, the ICP (intermediate capillary plexus) could not be clearly delineated on OCTA images, as shown in the Figure 3c image pair.
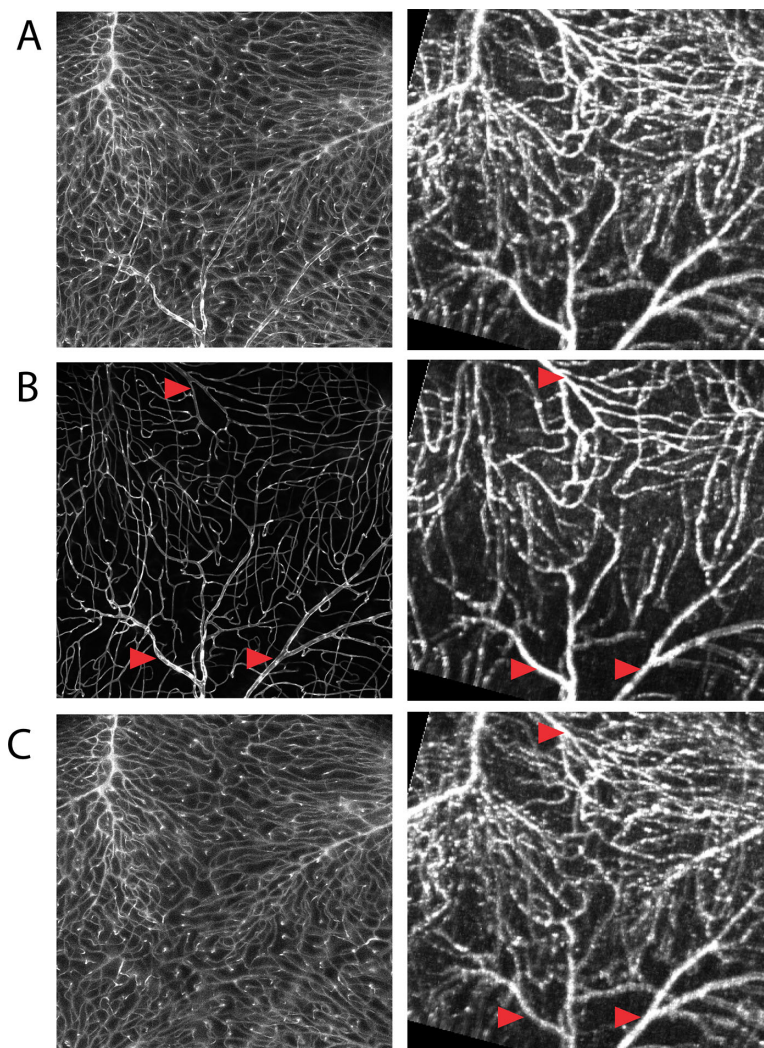
Figure 2. Corresponding pairs of maximum intensity projection images from a retinal region measuring 1270 μm × 1270 μm taken using confocal (*left column*) and OCTA (*right column*) technologies. (**A**) Full-thickness projection images of the confocal and OCTA stacks. Vessels from the superficial through to the deep vascular layer may be seen in this full-thickness projection. (**B**) The projected image pair from the top half of the stacks. (**C**) The projected image pair from the bottom half of the stacks. *Red arrowheads* point to retinal arterioles that are present in the top half of the confocal image stack. The same vessels are visible in the top half of the OCTA image stack, as well as the bottom half of the OCTA image stack as pointed out in (**C**), demonstrating the presence of projection artefacts.

## Data Generated from 2D Images After Processing

Comparison of Ridge Line Pixel Numbers

Figure 4 displays the tubeness images and the overlapping ridge line pixel image (after elastic co-registration) of the four capillary plexuses from one of the specimens. The matching pixels are shown in green in the middle panel.

The number of ridge line pixels obtained from the confocal and OCTA images provides evidence that there are fewer ridge line pixels in the OCTA images (one-way ANOVA, $P \leq 0.001$), indicating fewer tubular structures being detected on the corresponding OCTA images. Such underrepresentation of vessels on OCTA images is consistent across all four vascular layers (Table 1) and reflects the qualitative observation shown in Figure 3.

Table 1 presents the percentage of OCTA matching ridge line pixels to the confocal images. The highest number of matching ridge line pixels were from RPCN and SVP (superficial vascular plexus) with both layers having the respective highest match of 80 to 94% in some specimens. The number of matching pixels is the lowest for ICP ranging from 11% to 23% at the most. However, based on the lack of visually obvious structure matching, the quantitative matching pixels in ICP are more likely from projection artefacts than from
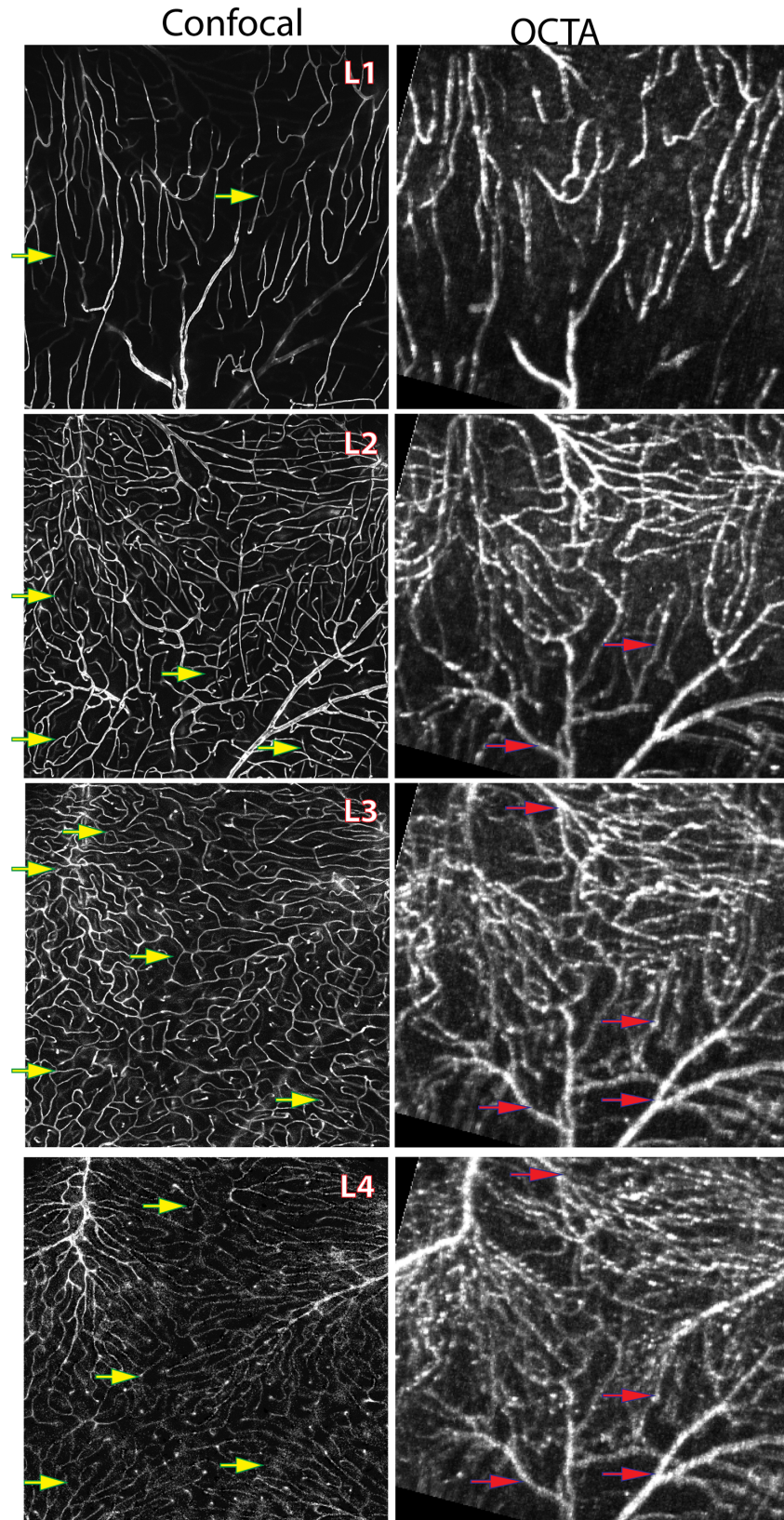
Figure 3. Four segmented vascular layers in 2D maximum local contrast projection images. The retinal microvasculature was segmented into four vascular layers according to retinal depth and pattern of vascular plexuses. The image stacks were segmented such that the stacks are continuous through the layers and that there was no overlap in the layer selection for either the confocal or OCTA stacks. Four distinct vascular layers are clearly seen in the 2D projection of confocal images. Projection artefacts from larger vessels located in more superficial

→

←
layers may be seen appearing in the deeper OCTA layers (*red arrows*). *Yellow arrows* point to examples of smaller vessels that are present in confocal images but missing from OCTA images. In particular, the third vascular layer could not be identified in OCTA image stack.
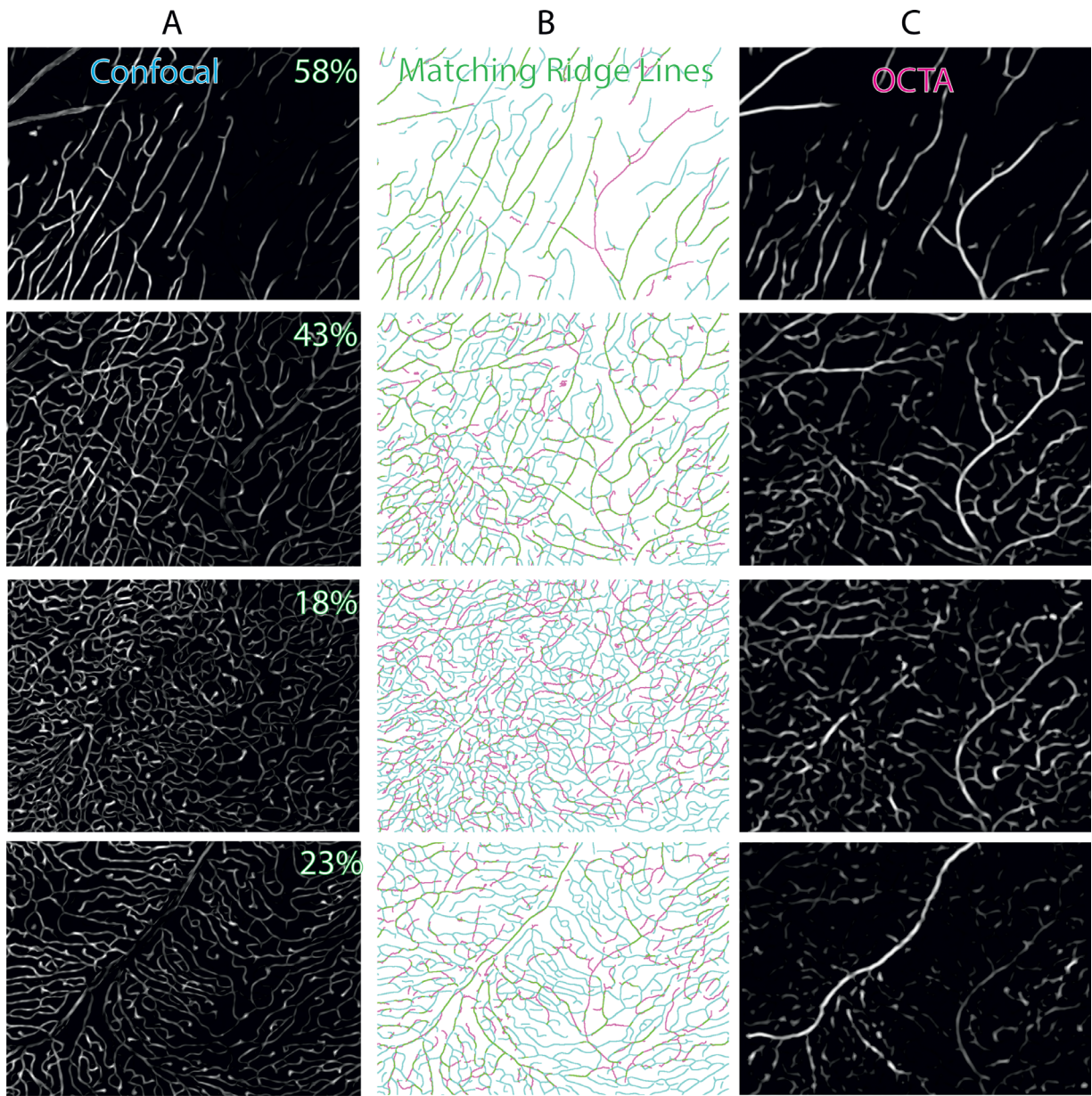
Figure 4. Matching ridge line pixels for the four vascular layers from one specimen. (A) The confocal images of the four layers after pre-processing to highlight the tubular structures. (C) The corresponding OCTA images of the four layers after pre-processing to highlight the tubular structures and scaling. (B) The ridge line pixels of the tubular structures from the confocal image superimposed on those of the OCTA image of the corresponding layer (after elastic registration of the OCTA ridge image to confocal ridge image). The confocal ridge line pixels are shown in *blue*, the OCTA in *pink*, and the overlapping matching pixels as *green*. The numbers shown are the percentage of matching pixels from the ridge line image pairs for each layer.

matching vessels. The DCP has a 15% to 30% range of matching pixels in the image pairs, mainly from larger draining venule present in this layer. The data provide evidence that the extent of matching in RPCN and SVP is greater than that in ICP and DCP ($P < 0.05$).

Vessel Density Using Grid Line Intercepts

Vessel density was also measured using the grid line intercepts method (Fig. 5) and the results shown in Table 2. Consistent with the observations from the ridge line pixel measurement method, the number of

Table 1. Percentage of OCTA Matching Ridge Line Pixels to Confocal (Mean ± SE (n))

	RPCN	SVP	ICP	DCP
% Matching ridge line pixels	51.2 ± 7.98 (6)	43.7 ± 6.50 (10)	17.7 ± 1.19 (10)	21.5 ± 1.68 (9)
% Vessel Pixel Confocal[*]	7.3 ± 2.56 (6)	10.7 ± 0.87 (10)	14.2 ± 0.56 (10)	13.1 ± 0.61 (9)
% Vessel Pixel OCTA[†]	1.9 ± 0.66 (6)	3.5 ± 0.38 (10)	7.1 ± 0.42 (10)	5.9 ± 0.64 (9)
P value (paired *t* test)[‡]	0.031	<0.001	<0.001	<0.001

[*]The number of ridge line pixel divided by the sum of all image pixels multiplied by 100%.
[†]The number of matching pixels divided by the number of confocal ridge pixels multiplied by 100.
[‡]Paired *t* test was conducted on the percentage vessel pixel values from corresponding confocal and OCTA image pairs.
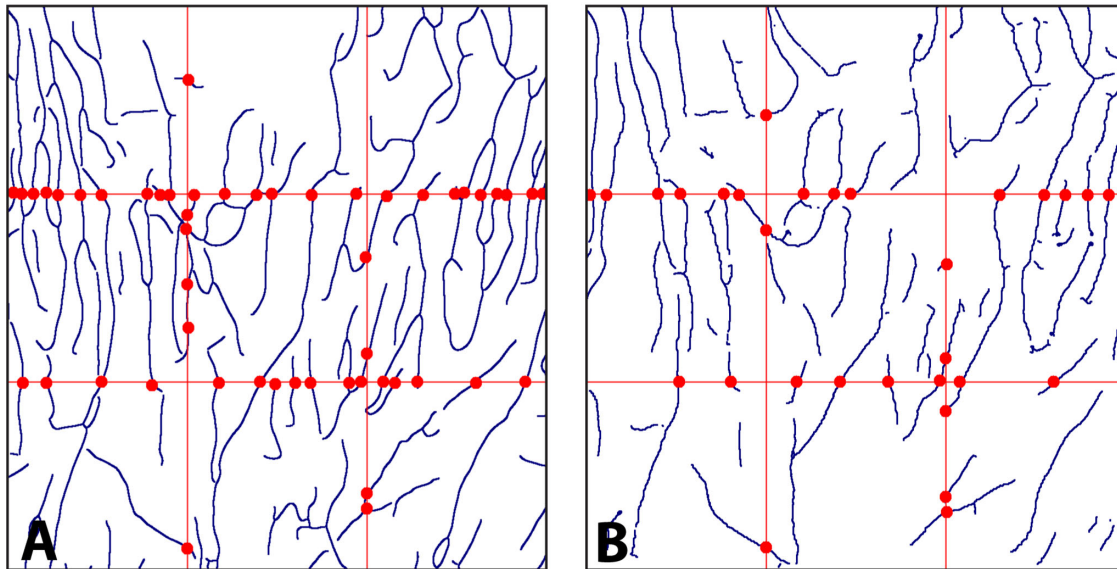
Figure 5. Grid line intercept method. This is a pair of ridge line confocal (**A**) and OCTA (**B**) images generated from layer 1 of the same specimen as shown in Figure 3. Two pairs of parallel and equally spaced *grid lines* were placed on the image and each vessel intercept recorded (indicated here as *red dots*). The number of intercepts from each image was recorded for analysis.

Table 2. Vessel Density in the Four Vascular Layers of Confocal and OCTA Images Expressed As the Number of Vessel Per 100 mm of Grid Line and ICD[*]

	Vessel Per 100 μm		ICD in μm	
Layers	Confocal	OCTA	Confocal	OCTA
RPCN (Mean ± SE, n)	1.02 ± 0.244, 6	0.47 ± 0.10, 6	133.53 ± 32.212, 6	261.69 ± 51.870, 6
SVP (Mean ± SE, n)	1.62 ± 0.191, 10	0.93 ± 0.09, 10	71.16 ± 9.550, 10	117.83 ± 11.031, 10
IVP (Mean ± SE, n)	1.74 ± 0.190, 10	1.11 ± 0.093, 10	65.92 ± 8.798, 10	95.46 ± 7.668, 10
DVP (Mean ± SE, n)	1.73 ± 0.192, 9	1.11 ± 0.136, 9	65.07 ± 8.844, 9	103.38 ± 15.285, 9

Data are presented as mean ± SE, number of specimen. ICD, intercapillary distance.
[*]ICD is an inversion of the vessel per 100 μm index.

vessel intercepts on OCTA images (mean of 0.95 ± 0.07, $n = 35$) and confocal images (mean of 1.58 ± 0.106, $n = 35$) provide evidence that there are fewer vessels on the corresponding OCTA images (paired *t*-test, *P* value ≤ 0.001). An analysis by layers provides evidence that there is a smaller vessel density on corresponding OCTA images at all layers (Table 2, paired *t*-test *P* values range from <0.001–0.016).
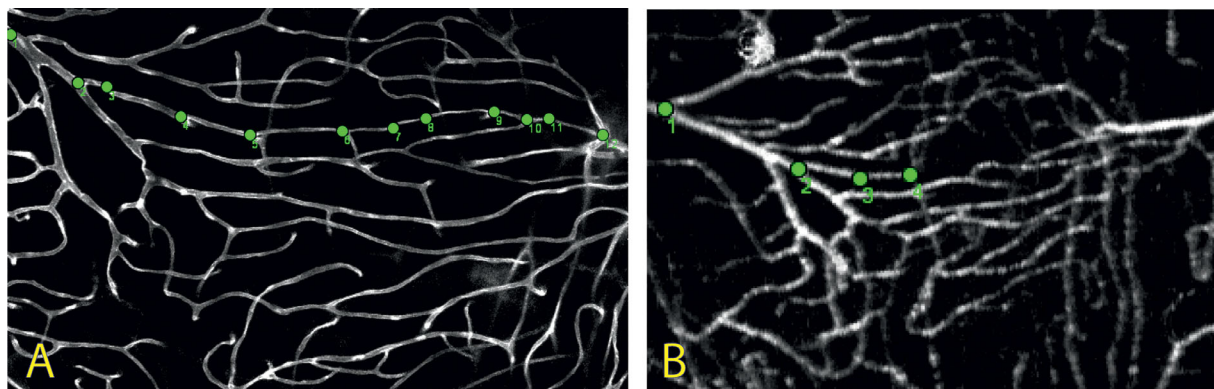
Figure 6. Vessel tracking through confocal (A) and OCTA (B) stacks using FIJI. Each image shown is actually a snapshot of a scrollable z-stack for which points can be placed at any *x, y,* and *z* position. An arteriole branch was tracked through the image stacks from arteriole side on the left to the venous drainage on the right. This vessel has a diameter of 7.73 μm at the point of branching from the main arteriole (dot point 2 on the confocal image) and can be tracked through a total depth of 13.75 μm for a total track distance of 572 μm within the SVL within the confocal stack. Total length on the OCTA stack, however, can only be tracked 338 μm through a depth of 16.5 μm and was not visible from mid-track onward (dot point 4 on the OCTA image).

Vessel Tracking

The regions selected for vessel tracking in 3D contained downstream branches from retinal arterioles. Arterioles branching off from the main retinal artery have a mean diameter of 26.6 ± 0.89 μm ($n = 10$) at the branch off point. The mean diameters and standard errors of the 10 arteriole and venule pairs within the 800×500 μm study region measured to be 21.0 ± 1.88 μm and 23.5 ± 3.99 μm respectively. The arteriole to venule mean linear distance (within the 10 study regions) is 769.2 ± 62.37 μm ($n = 10$), contained within an average confocal stack thickness of 110 ± 9.8 μm, $n = 10$.

Vessels were identified and matched by location and appearance across the confocal and OCTA study regions. Figure 6 shows an example of a vessel tracked using FIJI. Green dots were placed on the vessel being tracked on the corresponding confocal and OCTA 3D stacks. The 2D projection image is shown in this figure, but the tracking was done on the 3D z-stacks.

Vessel Track Measurements

Overall, 49 vessels were tracked across 10 porcine retinae. The tracks have a mean track length of 669.2 ± 30.98 μm ($n = 49$) as measured on confocal images and a mean visible length of 439.6 ± 43.3 μm ($n = 49$) on OCTA images. The data provide evidence that the track lengths visible on the OCTA images are shorter than the full tracks found on confocal images ($P < 0.001$). The number of branch points visible along the vessel track on OCTA images is 2.6 ± 0.28 ($n = 49$) and 5.5 ± 0.45 ($n = 49$) on confocal images. The data

provide evidence that the number of branch points is less for the OCTA images ($P < 0.001$). The retinal depth at which the visible portion of track traveled on OCTA is 20.0 ± 3.26 μm ($n = 49$) compared to 42.1 ± 3.20 μm ($n = 49$) for the corresponding confocal z-stack. The data provide evidence ($P < 0.001$) that this is shallower in the OCTA images. However, the diameter of the vessel at the end of track is not statistically significantly different between the confocal (7.01 ± 0.31 μm, $n = 49$) and OCTA track ends (7.40 ± 0.25, $n = 49$; $P = 0.168$).

The identification of missing vessels on OCTA corresponding to the vessel dive point and branch point prompted more detailed investigations using vessel tracking and quantification of the differences observed by grouping. Comparison of depth color-coded 2D projection of corresponding image stacks (Fig. 7) identified many vessels that are present on the confocal image but absent from OCTA image stack.

Analysis of Vessel Track Measurements Between Vessel Sub-Groups

Figure 8 shows examples of vessel subgroups by angle of descent and angle of dive. The angle of (vessel) descent and angle of dive (sharp downward turn) for each track was measured, and the mean value along with the range of angle measured presented in Table 3. The data provide evidence ($P < 0.05$) that group A vessels have flatter tracks within a shallow retinal depth, whereas group B and C vessels have a steeper descent into the deeper retina. They also provide evidence that there is a difference in the angles of vessel descent between the three groups (Dunn's test, $P < 0.001$). Finally, they provide evidence that there is a significant
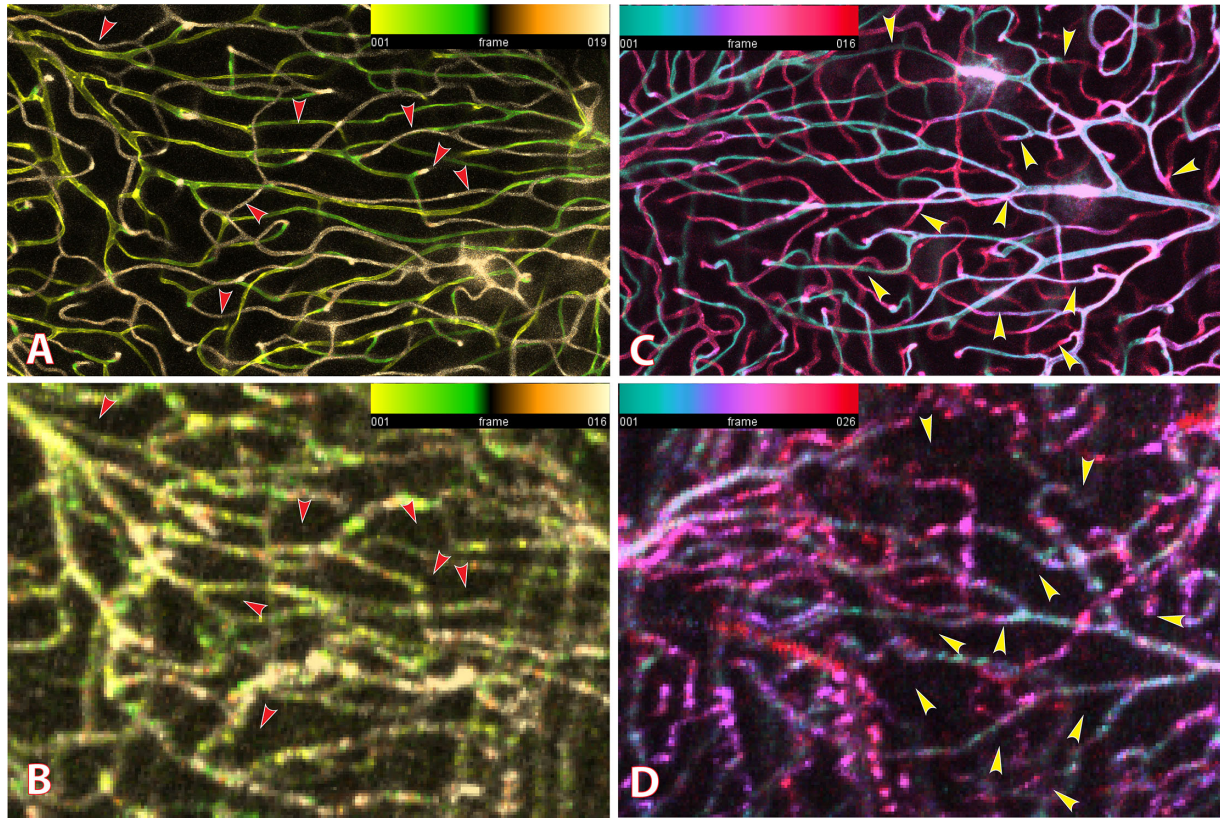
Figure 7. Depth color coded 2D maximum intensity projection of corresponding image stacks from regions of interest. (**A**, **B**) The respective confocal and OCTA 2D images from the same study region in the respective segmented stack. Both images were color coded according to depth (the color indicates the z-position at which the maximum intensity value occurs) as indicated by the *color scale bar* showing yellow-green vessels in the top half of the stack and brownish orange vessels in the lower half of the stack. *Red arrowheads* point to corresponding locations in the two stacks, showing vessels that were visible in the confocal image stack either branching from the top half of the stack or located in the bottom half of the stack but not visible on the OCTA images stack. (**C**, **D**) The respective confocal and OCTA 2D images from a study region of another eye. Both images were depth color coded using a green-blue-magenta-red scale as shown. *Yellow arrowheads* point to vessels that were visible in the confocal image stack but not visible on the corresponding OCTA stack. The vessels pointed out were either branching from the upper layers of the stack or in the deeper layers of the stack.

difference in the dive angle for vessels in group B and group C ($P < 0.001$).

Figure 9 shows an example of corresponding vessel tracks in the confocal and OCTA stacks from each group. Table 4A presents the mean ± standard error for the vessel track lengths and the number of branch points. Table 4B presents the mean ± standard error for the vessel track depth and vessel diameter for the corresponding vessels from confocal and OCTA study regions. Table 5A and 5B presents the percentage visibility of OCTA measurements compared to corresponding confocal images.

Vessel Track Lengths. Measurements of vessel track lengths are presented in Table 4A according to their groupings. There is no statistically significant difference in the full track lengths as measured on confocal images among the three groups ($P = 0.536$). There

is a statistically significant difference in the length of the visible part of the tracks on OCTA as measured using confocal images between the three groups ($P = 0.024$). The data provide evidence that group B OCTA visible track length is significantly shorter than group A (Holm-Sidak method comparing Group A vs. B, $P < 0.05$). They also provide evidence that the percentage track length visible on OCTA is different among the three vessel groups and that with group A is the most visible (Table 5A).

Branch Points. Data for counting of branch points are presented in Table 4A. There is a statistically significant difference between the number of branch points present on the tracks among the three groups ($P = 0.032$). The data provide evidence that there are more branch points present on group A vessels than group B vessels (Holm-Sidak method comparing Group A vs.
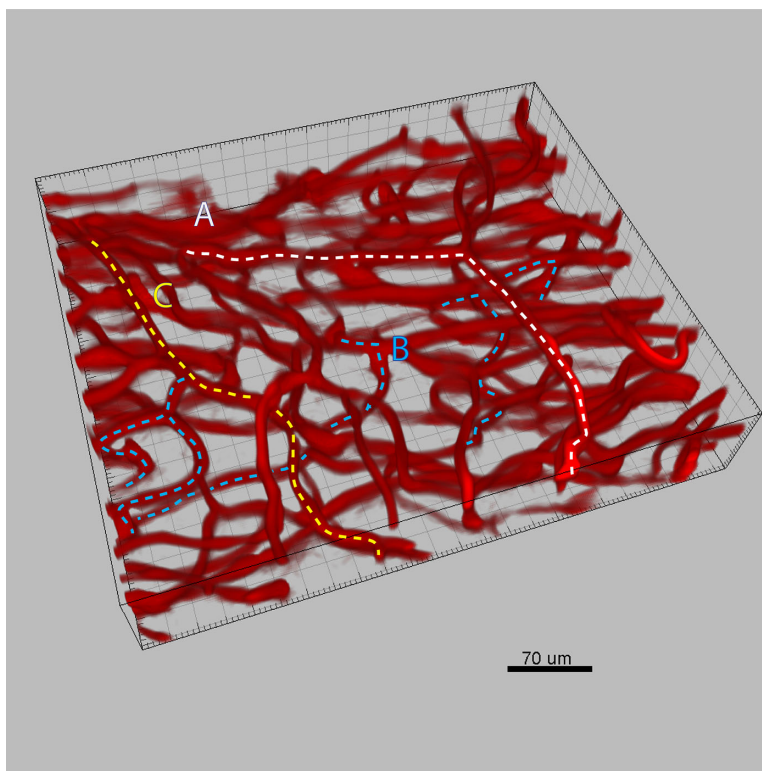
Figure 8. Illustrating the grouping of vessel track by angle of descent in a 3D projection of a small portion of a study region. Angle of descent refers to the steepness of vessel descent within the retina. (A) Group A vessels stay within 20 μm horizontal retinal thickness in its entire track. (B) Group B vessels have a sharp dive somewhere along the track into the deeper retina with a mean angle of 61.8°. (C) Group C vessels have a more gradual descent into the deeper retina and could contain a moderate dive of vessel track into the retina. Bounding box contains major grid mark at 50 μm.

Table 3. Characteristics of Vessel Tracks Grouping

Group	Angle of Descent (Mean ± SE, N)	Range of Angle of Descent	Track Dive Angle (Mean ± SE, N)	Range of Track Dive Angle
A	0.7° ± 0.18°, 12	0.132°–2.159°	N/A	N/A
B	12.9° ± 3.63°, 16	2.34°–53.19°	48.6° ± 3.95°, 16	26.6°–76.37°
C	5.7° ± 0.91, 21	1.85°–18.27°	29.1° ± 4.62°, 14	13.49°–67.60°
P values (ANOVA)	<0.001[*]		<0.001[*]	

[*]Statistical significance.

B branch point numbers, $P < 0.05$). However, there is no statistically significant difference in the number of branch points visible on OCTA between the vessel groups ($P = 0.113$). Overall, less than 50% of the branch points present on the confocal tracks are visible on the OCTA tracks (Table 5A). Moreover, there is no statistically significant difference in this percentage among the three groups ($P = 0.564$). More than a third of the vessel tracks in group B and half of the vessel tracks in group C are no longer visible at a branch point (Table 5B).

Vessel Track Depth. Table 4B presents the data for track depth measurements. The track depth is statistically significantly different among the three groups ($P < 0.001$). The data provide evidence that group A tracks are shallower when compared with than group B tracks ($P < 0.05$), mostly within the vitreal 20 μm of confocal retinal depth. However, there is no statistically significant difference between the retinal depths of visible OCTA tracks ($P = 0.602$) falling between 15 to 30 μm from the top. These results indicate that tracks are more likely
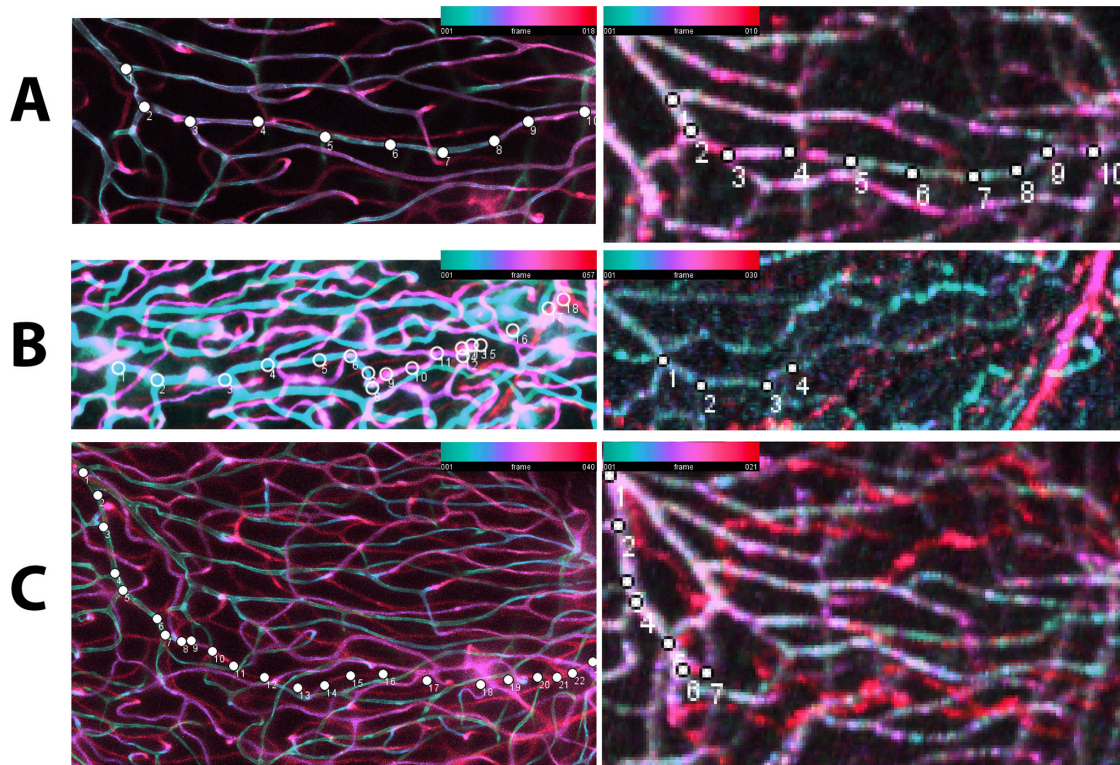
Figure 9. Representative track of each of the vessel subgroups **A**, **B**, and **C**. The corresponding confocal (*left*) and OCTA (*right*) stacks are color coded according to depth and placed side by side for direct comparison. The *white dots* and *circles* mark the vessel being tracked. Track A traveled its full course within 2 μm in retinal thickness, and the full track (dots 1 to 10) can be seen on the corresponding OCTA image. Track B traveled through 70 μm retinal depth with a sharp dive at position 8 as shown in the confocal projection image. The corresponding OCTA track was visible only to point 4 and the track lost at branch point. Track C traveled through 50 μm retinal depth with a moderate angle of descent. There is a dive in track angle at point 7, after which point, the OCTA signal was not present.

Table 4A. Mean Value for the Track Measurements According to Their Groupings

Group Name	Track Length–Confocal in μm	Track Length–OCTA in μm	No. of Branch Point Visible on Confocal (Holm-Sidak)	No. of Branch Point Visible on OCTA
A (Mean $\pm$ SE, n)	756.4 $\pm$ 55.23, 12	599.3 $\pm$ 70.04, 12	7.4 $\pm$ 0.96, 12	3.3 $\pm$ 0.43, 12
B (Mean $\pm$ SE, n)	666.0 $\pm$ 44.37, 19	307.6 $\pm$ 54.40,[*] 19	4.4 $\pm$ 0.59,[*] 19	1.9 $\pm$ 0.42, 19
C (Mean $\pm$ SE, n)	696.3 $\pm$ 63.27, 18	472.66 $\pm$ 86.12, 18	5.4 $\pm$ 0.77, 218	2.7 $\pm$ 0.55, 18
P value (ANOVA)	0.536	0.024[†]	0.032[†]	0.113

[*]Holm-Sidak method comparing Group A vs. B, $P < 0.05$.
[†]Indicate statistical significance ($P < 0.05$) between measurements from the three groupings as analysed by Oneway ANOVA.

to be visible if they are present in the superficial retina.

Vessel Diameter. Table 4B presents the vessel diameter measurements at the end of the visible vessel tracks. There is no statistically significant difference in the vessel diameter of the vessel tracks among the three groups ($P = 0.191$). Similarly, there is no statistically

significant difference in the vessel diameter at which the visible OCTA tracks stopped among the three groups ($P = 0.507$). These results indicate vessel diameter is not a determining factor in OCTA visibility.

Dive Angle. Some of the vessels in Group B and C have a region where the vessel turned sharply downward into the deeper retina. This region of the vessel is referred to

Table 4B. Mean Value for the Track Measurements According to Their Groupings

Group Name	Total Track Depth in μm Confocal	Total Track Depth in um for OCTA	Diameter of Vessel End of Track (Confocal) in μm	Diameter of Vessel End of Track (OCTA) in μm
A (Mean ± SE, n)	*15.8 ± 3.55, 12	14.3 ± 3.96, 12	6.3 ± 0.48, 12	7.0 ± 0.52, 12
B (Mean ± SE, n)	57.1 ± 4.65, 19	18.1 ± 6.33, 19	6.7 ± 0.39, 19	7.3 ± 0.45, 19
C (Mean ± SE, n)	43.9 ± 3.07, 18	26.0 ± 5.57, 18	7.9 ± 0.67, 18	7.7 ± 0.38, 18
P value (ANOVA)	<0.001[†]	0.602	0.191	0.507

[*]Dunn's Method of pairwise multiple comparison found Group A has a significantly different track depth from the other two gruops.

[†]Indicate statistically significantly difference ($P = < 0.001$) using Kruskal-Wallis One Way ANOVA.

Table 5A. Percentage of Visible Structures on OCTA Compared to the Corresponding Vessel Track on Confocal

Group	% Branch Point	% Track Length	% Track Depth
A (Mean ± SE, N)	47.0 ± 4.86, 12	81.5 ± 9.03, 12	87.6 ± 8.73, 12
B (Mean ± SE, N)	37.6 ± 6.83, 19	47.4 ± 7.94, 19	28.5 ± 8.73, 19
C (Mean ± SE, N)	45.9 ± 7.86, 18	59.7 ± 9.54, 18	54.9 ± 11.33, 18
P value (ANOVA)	0.564	0.015[*]	0.001[*]

[*]Indicates a statistically significant difference among the groups with P value less than 0.05 as analysed by One Way ANOVA.

Table 5B. Percentage of Visible Structures on OCTA Compared to the Corresponding Vessel Track on Confocal

Group	Full Track (%)	Partial Track (%)	Track Totally Missing (%)	% Track Missing at a Branch Point
A	66.66	33.33	0.00	25.00
B	15.79	73.68	11.11	36.84
C	38.89	44.44	16.67	50.00

Table 6. Dive Angle of Vessels in Groups B and C

Groups	Dive Angle	Confocal Track Length After Dive	OCTA Track Length After Dive
B (Mean ± SE, N)	50.6 ± 3.30, 19	368.7 ± 54.61, 19	64.8 ± 38.09, 19
C (Mean ± SE, N)	18.8 ± 2.06, 12	464.6 ± 88.52, 12	248.7 ± 86.24, 15
P value (ANOVA)	<0.001[*]	0.286	<0.001[*]

[*]Indicates a statistically significant difference, with P value less than or equal to 0.001, among the groups as analysed by One Way ANOVA.

as the diving part and the angle of downturn the dive angle. Table 6 display the data to provide evidence that the dive angle is sharper in group B vessels compared to group C ($P < 0.001$), and the length of visible OCTA track after the point of dive is shorter in group B vessels compared to group C vessels. This indicates the angle of dive to be an important factor in OCTA visibility.

Discussions

Direct comparison of OCTA images against vascular histology on of the same retinal region acquired using confocal microscopy is one of the most reliable ways to validate the OCTA techniques. With carefully designed postprocessing of 2D projection images, vessel tracking on 3D image stacks, and data analysis, we have found similarities and differences of the retinal capillary network between OCTA images and confocal images. We believe such information is useful for validating current OCTA techniques and will contribute to developing better OCTA techniques in the near future.

The major findings from this study are the following: (1) There is a good representation of the larger caliber vessels (usually larger than 10 μm) of the retinal capillary network in the SVP and DCP on the OCTA image stacks. (2) There is an underrepresentation of the

smaller retinal microvessels less than 10 μm in diameter and branch points on OCTA images in all four retinal vascular plexuses, being most severe in the ICP. (3) An increase in the angle of descent of a vessel track is associated with reduced visibility on OCTA. (4) There is a tendency for the visibility of a vessel track to be lost on OCTA at a branch point or during a sharp dive. (5) There is a reduction in visibility with increase in retinal depth of the vessel track.

There are some significant benefits in the model used in this study, including the following: (1) Similarities of the porcine eye to the human eye, notably in terms of anatomical parameters such as the size of the globe, the presence of a holangiotic and radiating vascular pattern from the optic disc, the organization of retinal vessels into three to four vascular plexuses, and an avascular outer retina. This makes it a comparable experimental model to further understanding of the retinal microvasculature with relevance to the human eye. (2) The availability of fresh porcine eyes, ability to perfuse the retinal microvasculature, and direct comparison of the exact retinal area used for OCTA image acquisition against high-resolution confocal images from histologically perfusion-labeled specimens makes it a good model for direct validation of current OCTA technology. (3) Confocal microscopy of perfuse-labeled retinal microvasculature is a well-established technique that allows specific labeling and viewing of the entire retinal vasculature within the intact retina. The combination of a high-quality objective lens, use of phosphorescence stable probes, and motorized precision stage movement control enabled acquisition of vascular information in high-pixel resolution in the x, y, and z axes to the level of micrometers. Detailed information on the distribution, topographically and at a cellular level, of the microvasculature may be obtained for analysis and quantitation making available a gold standard and reference point against which data obtained from images of live subjects may be compared against. (4) Importantly this model eliminates motion artefacts that are a major source of artifacts in OCTA.

Although OCTA images and confocal images were acquired from the same region, the quantitation of their similarities and differences was not straightforward. To effectively avoid potential bias, we have carefully considered and selected the two approaches for quantitation. Both OCTA and confocal microscopy are acquired 3D volume images. Confocal images were acquired using high-resolution confocal microscopy and the intact retinal capillary network from confocal images can be considered a gold standard to validate OCTA images. Such high-resolution images without imaging artefacts cannot be obtained using current OCTA technique. The two approaches involved postprocessing of 2D projection images and vessel tracking on 3D image stacks. Segmentation was applied to divide the retinal capillary plexus into RPCN, SVP, ICP, and DCP as previously reported.[28,29]

Given that the signal from the OCTA images is from moving red blood cells, the caliber size of the capillary network may not represent the exact size. This is further exacerbated by the spot size of the imaging beam used for OCTA being larger than the smaller capillaries. The pixel resolution of OCTA images is between 3.85 to 4.14 μm per pixel, which is more than threefold lower than that of confocal images at 1.24 μm per pixel. The large pixel size on OCTA images is the likely cause for the significantly larger vessel diameters when compared to measurements obtained from histology images from human donor eyes.[10–12] The lower resolution of OCTA images may also have contributed to masking of signal from underlying smaller microvessels, especially where there is strong projection artifacts from layers above.

The shadow projection artifacts in OCTA images from larger and more anteriorly situated vessels made clear delineation of underlying smaller vessels impossible to discern; hence, coregistration across the 3D stacks was impossible to achieve. 2D projections of vascular layers also suffer from projection artefacts but sufficient correspondence was present for landmark registrations, enabling elastic transformation of the OCTA images to correct distortions resulting from porcine eye curvature, refractive error and orientation differences. Hence, the 2D projection images were used for quantitating vessel density. Moreover, severalfold difference exists in the pixel resolution of confocal and OCTA images. Quantitation of vessel density would therefore not be accurate if it was based on a percentage area occupation calculation. Therefore we have applied a multi-scale tubeness filter (based on eigenvalues of the Hessian matrix) on the raw confocal and nonlocal means-filtered OCTA images to highlight the vessels. To include vessels of all sizes, we determined the optimum range of size scales for inclusion (pixelwise maximum) in the final tubeness images. Five scale sizes were used for confocal images and two for OCTA images. Vessel centerlines/ridges (single pixel thick) were then then computed for the resulting tubeness images using the same parameters applied to both sets of images. The comparison of ridge line pixels generated from the raw image files therefore enabled a more accurate representation of the relative vessel density between the two techniques than would be possible if quantitation was based on area occupation measurement.

The quantitation by ridge line pixel numbers provided an index for the relative presence of tubular

structures which is an accurate reflection of what can be observed qualitatively by eye. The grid line intercept methods provided an index for vessel density that is higher than the values obtained from the perifoveal[32] and the peripheral retina[30,33] of human specimens. It is known that the foveal region[9] has a denser vascular distribution than that of the perifoveal region[32] in the human retina. Although the pig eye does not have a fovea, the area centralis[34,35] is macula-like and contains the highest concentration of ganglion cells[35] and can reasonably be expected to have a denser vascular distribution as shown in our current study.

Our results suggest that weak OCTA signals occur in situations such as smaller size caliber vessels, increase in the angle of descent of a vessel, and at a branch points or during a sharp dive. These results could be due to the limitations of OCTA technical aspects and also can be contributed by biological aspects. Weak OCTA signal could be induced by the properties of the retinal microcirculation. The microcirculation can be defined by the size of the blood vessels, but more importantly it has specific rheologic properties that differ significantly from those in the large vessels.[36] In the smaller vessels, particularly in vessels less than 100 μm luminal diameter, an important hemodynamic feature, the Fahraeus-Lindqvist effect, occurs in the microcirculation, which leads to diameter-dependent reduction of hematocrit and effective blood viscosity. This means that there are much fewer red blood cells along with larger plasma gaps in the smaller retinal capillaries. In fact, the capillary caliber is only 5 to 7 μm and usually smaller on the arteriolar side. It is possible that weak OCTA signal could result from smaller capillaries where there are fewer red blood cells and larger plasma gaps. In addition, the topographic distribution of the vasculature could also significantly contribute to blood flow and hematocrit distribution.[37]

We have previously studied the topography of human retinal vasculature particularly in the macular region and gained detailed information about the pattern, caliber, branches (numbers, orders, generations, and angles).[16,38] More importantly active regulation are in play in the retinal vasculature having a critical role in allowing blood supply to match high metabolic demands of the retinal neurons spatially and temporally.[36] Such active regulation does not only occurred in the arterioles but in the capillaries.[39,40] Therefore one should never expect OCTA signal at the capillary level to be identical between acquisitions. The vessel signal used for analysis in this study was an averaged signal from 20 OCTA volumes. The isolated arterially perfused eye preparation has eliminated the motion artefacts, and the custom-built OCTA device has a short acquisition time allowing us to take multiple volumes and average. The averaging could have a cancelling effect on those vessels that have a lower viscosity, fewer red blood cell movements, and, hence, give a weak or nil OCTA signal in any given single frame.

Another important and interesting finding from our study is that we noted that sharply diving vessels, such as those in group B, are often not visible on the OCTA or that visibility is lost after the dive. The presence of these diving vessels between the capillary plexus are likely consequences from retinal vessel development processes. In both the porcine and human eyes, the deeper vascular plexuses begin as "budding" or "sprouting" from blood vessels of the inner vascular plexus. Such tip/stalk developments are observed to sprout from the venous side of the superficial plexus and penetrate into the deeper retina in a perpendicular fashion.[41,42] The presence of numerous perpendicular branches connecting the capillary layers in porcine and human retina are well documented.[18,33] Such perpendicular branches that can be seen in our porcine specimens have also been previously reported by Fouquet et al.[43] Such perpendicular branches are believed to be an important feature for the retina because the eye is an optical organ that requires minimal optical disruption from the retinal vasculature. There is currently no quantitative data to indicate whether there is a difference in the relative proportion of the existence of such perpendicular vessels in the porcine and human eyes. The availability of such quantitative data could help to explain the difference in the percentage of vessels visible in OCTA in human and porcine eyes.

Our current study using the isolated porcine eye as the study model demonstrated that the intermediate capillary plexus that is present on histology is not visible on OCTA images. Whereas the major retinal vessels and many of their branches are clearly visible on OCTA images, more than half the branch points, branches and microvessels visible on confocal images are not visible on OCTA. Although there are many similarities between the human and the porcine eye in the anatomical lay out of vascular plexuses, there are several anatomical differences that could have contributed to the difference in OCTA imaging results obtained from the two species.

Unlike the human retina, which is supplied by a single central retinal artery, the porcine retina receives blood supply from several chorioretinal arteries. The singular arteriole supply and singular venular exit in the human retina ensures complete perfusion of the entire retinal microvasculature. The porcine retinal microvasculature, on the other hand, receives multiple arteriole supplies and so there is a possibility that the vessels imaged were not well perfused in our specimens.

An argument against this as a contributing cause of missing signal is that the perfusion labeling of the retinal microvasculature used the exact same vessel as cannulated for perfusion of red blood cells, with the confocal images demonstrating labeled vessels (hence, perfused) that are not visible on the OCTA images. In addition, as seen from the vessel tracking, a lot of vessels were visible on OCTA at the start of the track but lost signal on branching or diving deeper into the retina, indicating that the vessel was perfused to start with.

Second, the deeper layers of the porcine retinal microvasculature are predominantly venous in nature and receives supply from branches of the SVP.[18] The IPV is noted to be predominantly capillaries in caliber and predominantly venous. In the human retina, however, the ICP receives arteriole supplies from third- or fourth-order arterioles coming from the main retinal arteries or direct second-order arteriole supply from the main retinal arteries.[44] This difference in the origins of the capillaries in the ICP and the small vessel caliber may be a contributing factor to OCTA visibility.

The speckle variance detection method in the current system could have limited the visibility of vessels that are diving steeply into the retina. The current system as an intensity-based speckle variance detection system is able to detect sideway movements of red blood cells as speckle variation. The near-perpendicular travel of red blood cells in a vessel of relatively small caliber could have resulted in a relatively slower red blood cell movement that is away from the laser beam, limiting their visibility. A recent study also showed that the asymmetry in the shape of red blood cells, as well as their alignment in shear flow, are important contributors to the visibility of capillaries in OCTA.[4,5,45]

OCTA is a useful, fast, and noninvasive technological advancement to the conventional retinal imaging techniques of color fundus photography and fluorescein angiography. Despite known limitations of projection artifacts and functional applications for accurate flow rate estimation, OCTA offers a way to investigate the retinal microvasculature in three dimensions in a way that was not possible in live subjects previously. This study has identified steeply diving branches or vessel track and the deeply seated small capillaries draining toward retinal veins to be problematic for OCTA visibility in the porcine retinal microvasculature. The functional importance of these vertical vessel segments in supplying the deeper retinal layers in the human macula has been shown in our recent article.[44] However, it is not known what percentage of these perpendicularly diving vessels may have been missed in the current clinical investigation of normal physi-ological and pathological retinal conditions. It would be worthwhile to conduct further investigations to find out the relative proportions of these perpendicular diving vessels in the human retina and if their visibility on OCTA has been compromised.

Acknowledgments

References

1. Kashani AH, Chen CL, Gahm JK, et al. Optical coherence tomography angiography: A comprehensive review of current methods and clinical applications. *Prog Retin Eye Res*. 2017;60:66–100.
2. Nikolopoulou E, Lorusso M, Micelli Ferrari L, et al. Optical coherence tomography angiography versus dye angiography in age-related macular degeneration: sensitivity and specificity analysis. *Biomed Res Int*. 2018;2018:6724818.
3. Or C, Sabrosa AS, Sorour O, Arya M, Waheed N. Use of OCTA, FA, and ultra-widefield imaging on quantifying retinal ischemia: a review. *Asia Pac J Ophthalmol*. 2018;7:46–51.
4. Enders C, Lang GE, Dreyhaupt J, Loidl M, Lang GK, Werner JU. Quantity and quality of image artifacts in optical coherence tomography angiography. *PLoS One*. 2019;14:e0210505.
5. Holmen IC, Konda SM, Pack JW, et al. Prevalence and severity of artifacts in optical coherence tomographic angiograms. *JAMA Ophthalmol*. 2020;138:119–126.
6. Lupidi M, Coscas F, Cagini C, et al. Automated quantitative analysis of retinal microvasculature in normal eyes on optical coherence tomography angiography. *Am J Ophthalmol*. 2016;169:9–23.
7. Gadde SG, Anegondi N, Bhanushali D, et al. Quantification of vessel density in retinal optical coherence tomography angiography images using local fractal dimension. *Invest Ophthalmol Vis Sci*. 2016;57:246–252.

8. Shahlaee A, Samara WA, Hsu J, et al. In vivo assessment of macular vascular density in healthy human eyes using optical coherence tomography angiography. *Am J Ophthalmol*. 2016;165:39–46.

9. Yu PK, Mammo Z, Balaratnasingam C, Yu DY. Quantitative study of the macular microvasculature in human donor eyes. *Invest Ophthalmol Vis Sci*. 2018;59:108–116.

10. Tan PEZ, Yu PK, Yang H, Cringle SJ, Yu DY. Regional differences in endothelial cell cytoskeleton, junctional proteins and phosphorylated tyrosine labeling in the porcine vortex vein system. *Exp Eye Res*. 2018;172:36–44.

11. Chan G, Balaratnasingam C, Xu J, et al. In vivo optical imaging of human retinal capillary networks using speckle variance optical coherence tomography with quantitative clinico-histological correlation. *Microvasc Res*. 2015;100:32–39.

12. Yu PK, Balaratnasingam C, Xu J, et al. Label-free density measurements of radial peripapillary capillaries in the human retina. *PLoS One*. 2015;10:e0135151.

13. Mammo Z, Balaratnasingam C, Yu PK, et al. Quantitative noninvasive angiography of the fovea centralis using speckle variance optical coherence tomography. *Invest Ophthalmol Vis Sci*. 2015;56:5074–5086.

14. Mammo Z, Heisler M, Balaratnasingam C, et al. Quantitative optical coherence tomography angiography of radial peripapillary capillaries in glaucoma, glaucoma suspect, and normal eyes. *Am J Ophthalmol*. 2016;170:41–49.

15. Balaratnasingam C, An D, Sakurada Y, et al. Comparisons between histology and optical coherence tomography angiography of the periarterial capillary-free zone. *Am J Ophthalmol*. 2018;189:55–64.

16. Yu DY, Su EN, Cringle SJ, Yu PK. Isolated preparations of ocular vasculature and their applications in ophthalmic research. *Progr Retinal Eye Res*. 2003;22:135–169.

17. Yu DY, Yu PK, Balaratnasingam C, Cringle SJ, Su EN. Microscopic structure of the retina and vasculature in the human eye. In: Méndez-Vilas A, Díaz J, eds. *Microscopy: science, technology, applications and education*. Norristown, PA: Formatex Research Center; 2010:867–875.

18. Simoens P, De SL, Lauwers H. Morphologic and clinical study of the retinal circulation in the miniature pig. A: morphology of the retinal microvasculature. *Exp Eye Res*. 1992;54:965–973.

19. Sanchez I, Martin R, Ussa F, Fernandez-Bueno I. The parameters of the porcine eyeball. *Graefes Arch Clin Exp Ophthalmol*. 2011;249:475–482.

20. Yu PK, Yu D, Alder VA, Seydel U, Su E, Cringle SJ. Heterogeneous endothelial cell structure along the porcine retinal microvasculature. *Exp Eye Res*. 1997;65:379–389.

21. Ju MJ, Heisler M, Athwal A, Sarunic MV, Jian Y. Effective bidirectional scanning pattern for optical coherence tomography angiography. *Biomed Opt Express*. 2018;9:2336–2350.

22. American National Standard Institute I. *American national standard for the safe use of lasers*. Orlando, FL: Laser Institute of America; 2014.

23. Zhang A, Zhang Q, Chen CL, Wang RK. Methods and algorithms for optical coherence tomography-based angiography: a review and comparison. *J Biomed Opt*. 2015;20:100901.

24. Lee S, Fallah N, Forooghian F, et al. Comparative analysis of repeatability of manual and automated choroidal thickness measurements in nonneovascular age-related macular degeneration. *Invest Ophthalmol Vis Sci*. 2013;54:2864–2871.

25. Yu PK, Balaratnasingam C, Morgan WH, Cringle SJ, McAllister IL, Yu DY. The structural relationship between the microvasculature, neurons, and glia in the human retina. *Invest Ophthalmol Vis Sci*. 2010;51:447–458.

26. Yu PK, An D, Balaratnasingam C, Cringle SJ, Yu DY. Topographic distribution of contractile protein in the human macular microvasculature. *Invest Ophthalmol Vis Sci*. 2019;60:4574–4582.

27. Schindelin J, Arganda-Carreras I, Frise E, et al. Fiji: an open-source platform for biological-image analysis. *Nature Methods*. 2012;9:676–682.

28. Cuenca N, Ortuno-Lizaran I, Sanchez-Saez X, et al. Interpretation of OCT and OCTA images from a histological approach: clinical and experimental implications. *Prog Retin Eye Res*. 2020;100828.

29. Spaide RF, Fujimoto JG, Waheed NK, Sadda SR, Staurenghi G. Optical coherence tomography angiography. *Prog Retin Eye Res*. 2018;64:1–55.

30. Tan PE, Balaratnasingam C, Xu J, et al. Quantitative comparison of retinal capillary images derived by speckle variance optical coherence tomography with histology. *Invest Ophthalmol Vis Sci*. 2015;56:3989–3996.

31. Arganda-Carreras I, Sorzano COS, Marabini R, Carazo JM, Ortiz-De-Solorzano C, Kybic J. Consistent and elastic registration of histological sections using vector-spline regularization. *Comp Vis Approaches Med Image Analysis*. 2006;4241:85–95.

32. Chan G, Balaratnasingam C, Yu PK, et al. Quantitative morphometry of perifoveal capillary

networks in the human retina. *Invest Ophthalmol Vis Sci*. 2012;53:5502–5514.

33. Tan PE, Yu PK, Balaratnasingam C, et al. Quantitative confocal imaging of the retinal microvasculature in the human retina. *Invest Ophthalmol Vis Sci*. 2012;53:5728–5736.

34. Chandler MJ, Smith PJ, Samuelson DA, MacKay EO. Photoreceptor density of the domestic pig retina. *Vet Ophthalmol*. 1999;2:179–184.

35. Hebel R. Distribution of retinal ganglion cells in five mammalian species (pig, sheep, ox, horse, dog). *Anatomy Embryol*. 1976;150:45–51.

36. Yu D-Y, Cringle SJ, Yu PK, et al. Retinal capillary perfusion: spatial and temporal heterogeneity. *Progr Retinal Eye Res*. 2019;70:23–54.

37. Tuma RF, Duran WN, Ley K. *Handbook of physiology: microcirculation*. 2nd ed. San Diego: Academic Press (Elsevier); 2008.

38. Yu DY, Yu PK, Cringle SJ, Kang MH, Su EN. Functional and morphological characteristics of the retinal and choroidal vasculature. *Prog Retin Eye Res*. 2014;40:53–93.

39. Attwell D, Buchan AM, Charpak S, Lauritzen M, Macvicar BA, Newman EA. Glial and neuronal control of brain blood flow. *Nature*. 2010;468:232–243.

40. Alarcon-Martinez L, Villafranca-Baughman D, Quintero H, et al. Interpericyte tunnelling nanotubes regulate neurovascular coupling. *Nature*. 2020;585(7823):91–95.

41. Selvam S, Kumar T, Fruttiger M. Retinal vasculature development in health and disease. *Prog Retin Eye Res*. 2018;63:1–19.

42. De Schaepdrijver L, Simoens P, Lauwers H. Development of the retinal circulation in the pig. *Anatomy Embryol*. 1995;192:527–536.

43. Fouquet S, Vacca O, Sennlaub F, Paques M. The 3D retinal capillary circulation in pigs reveals a predominant serial organization. *Invest Ophthalmol Vis Sci*. 2017;58:5754–5763.

44. An D, Yu P, Freund KB, Yu DY, Balaratnasingam C. Three-dimensional characterization of the normal human parafoveal microvasculature using structural criteria and high-resolution confocal microscopy. *Invest Ophthalmol Vis Sci*. 2020;61:3.

45. Bernucci MT, Merkle CW, Srinivasan VJ. Investigation of artifacts in retinal and choroidal OCT angiography with a contrast agent. *Biomed Opt Express*. 2018;9:1020–1040.

translational vision science & technology